Published in final edited form as:
Biomaterials. 2012 November ; 33(33): 8477–8485. doi:10.1016/j.biomaterials.2012.06.082.

Small molecule fluorophore and copolymer RGD peptide conjugates for *ex vivo* two-photon fluorescence tumor vasculature imaging

Alma R. Morales[a], **Ciceron O. Yanez**[a], **Yuanwei Zhang**[a], **Xuhua Wang**[a], **Sanchita Biswas**[a], **Takeo Urakami**[b], **Masanobu Komatsu**[b], and **Kevin D. Belfield**[a,c,*]

[a]University of Central Florida, Department of Chemistry, P.O. Box 162366, Orlando, FL 32816-2366, USA

[b]Sanford-Burnham Medical Research Institute at Lake Nona, 6400 Sanger Rd., Orlando, FL 32827, USA

[c]CREOL, College of Optics and Photonics, University of Central Florida, P.O. Box 162366, Orlando, FL 32816-2366, USA

Abstract

We report the use of small molecule and block copolymer RGD peptide conjugates for deep *ex vivo* imaging of tumor vasculature in "whole" excised tumors using two-photon fluorescence microscopy (2PFM). The fluorescent probes were administered to mice via tail-vein injection, after which the tumors were excised, fixed, and imaged without further sample preparation. Both RGD conjugates demonstrated specific targeting to tumor blood vessels, and this selectivity imparted excellent contrast in 2PFM micrographs that captured high-resolution 3-D images of the tumor vasculature up to depths of 830 μm in Lewis Lung Carcinoma (LLC) tumors. 2PFM *ex vivo* fluorescence micrographs clearly revealed tumor vessels, while differences in the sensitivity of tumor vessel imaging were apparent between the small molecule and block copolymer conjugates. Both the small molecule and polymer-based two-photon absorbing probe conjugate are valuable for deep tissue tumor microvasculature imaging.

Keywords

RGD peptide conjugates; Two-photon absorption; Fluorescent dyes; Copolymer probe; Two-photon fluorescence microscopy; Tumor vasculature

1. Introduction

The cell adhesion protein $\alpha_v\beta_3$ integrin is, in many ways, a very good biomarker for angiogenesis. It is highly expressed by activated endothelial cells of angiogenic blood vessels as well as many types of malignant tumor cells whereas it is not readily detectable in resting endothelial cells or in normal tissues [1]. Clinical studies have shown that the expression of $\alpha_v\beta_3$ integrin correlates with tumor grade [2,3], suggesting $\alpha_v\beta_3$ integrin as a biomarker for tumor malignancy. Therefore, the capability to detect $\alpha_v\beta_3$ integrin expression by a noninvasive imaging technology would allow better characterization of tumors and identify tumor regions with higher degrees of aggressiveness. Integrin inhibitors,

---

[*] Corresponding author. University of Central Florida, Department of Chemistry, P.O. Box 162366, Orlando, FL 32816-2366, USA. belfield@ucf.edu (K.D. Belfield).

that target $\alpha_v\beta_3$ integrin, have been created and have been evaluated in clinical trials as antiangiogenic therapeutics [4,5]. Additionally, many integrins, including those containing the α_v subunit, as well as $\alpha_{5\beta1}$ and $\alpha_{iib}\beta_3$ integrins, recognize Arg–Gly–Asp (RGD) motif found in extracellular matrix protein [6].

Linear [7,8], and cyclic RGD peptides [9] have been tested to target $\alpha_v\beta_3$ integrin for various purposes. Cyclic RGD peptides have been shown to better resist proteolysis and have a higher affinity and selectivity to the target integrins than their linear counterparts [10,11].

The diverse applications for RGD peptides include inhibiting apoptosis, angiogenesis, and tumor formation, coating surfaces for use as biomaterials, enhancing drug delivery, and imaging for diagnostic purposes. Cyclo (Arg–Gly–Asp–D–Phe–Lys) can be functionalized with various linker molecules through the amino group on the lysine residue. An RGD peptide has been functionalized with polyethylene glycol to enhance binding to liposomes for targeted drug delivery, resulting in effective tumor regression [12]. A number of cyclic RGD conjugates have been developed, for instance, with radionuclide-chelating agents for target-specific cancer imaging [13–17]. Other RGD conjugates include metallic nanoparticles, quantum dots [18,19], and near-infrared (NIR) fluorochromes [20–22].

Multimeric RGD peptide motifs have even superior activity to monomeric analogs in targeting integrins [23–25]. Carrier systems such as liposomes, nanoparticles, proteins, and other polymers bearing multiple RGD-peptides are often more likely to be internalized via receptor-mediated endocytosis than single peptide constructs. Synthetic and natural polymers can be attached with multiple copies of an RGD peptide and a drug or fluorescent probe, affording multivalent binding and internalization.

Other common advantages attributable to RGD attached to macromolecular carriers include higher affinity and internalization facilitated by multivalent RGD-ligands and reduced renal filtration since the higher molecular size of the carrier prevents glomerular filtration. This may lead to prolonged blood circulation times and longer presentation of the ligand to target receptors within tissue [26]. The high molecular weight of most carriers leads to passive retention in a tumor via the so-called enhanced permeability and retention (EPR) effect.

Line et al. reported *N*-(2-hydroxypropyl) methacrylamide (HPMA) copolymer-based conjugates of mono-(RGDfK) and doubly cyclized (RGD4C) peptides labeled with ^{99m}Tc and ^{111}In [27]. These conjugates delivered diagnostic and therapeutic agents effectively and selectively due to their multivalency, target specificity, passive tumor localization, and extravascularization activity. A cyclic RGD dimer with two tetra(ethylene glycol) (PEG 4) linkers was labeled with the fluorescent near-IR dye IRDye800 and investigated whether the RGD dimeric probe with PEG 4 spacers showed better tumor-targeting properties than the RGD dimer without PEG 4 spacers. *In vivo* near-infrared fluorescence (NIRF) imaging revealed higher tumor accumulation and tumor to background contrast of the probe with PEG 4 than the probe without PEG 4, ascribed to increased receptor binding affinity [28].

K. Chen et al. have developed a PEGylated amphiphilic triblock copolymer to coat iron oxide nanoparticles. A cyclic RGD along with an NIR dye IRDye800, were covalently coupled onto the triblock copolymer coated nanoparticles for tumor targeting and MR imaging [29]. The nanoconjugates showed excellent tumor targeting efficiency, relatively long circulation half-life and limited liver macrophage engulfment, which was attributed to their compact hydrodynamic size and PEGylated coating.

Fluorescence-based molecular imaging is becoming increasingly important, due, in large part, to the development of highly sensitive cameras and the increasingly higher spatial resolution that can be achieved [30,31]. However; fluorescence signals have limited tissue penetration making quantitative biodistribution analysis difficult. Two-photon fluorescence microscopy (2PFM) has proven effective in observing cellular events deep inside the tissue. 2PFM typically employs simultaneous absorption of two near-infrared (NIR) photons, which provides a number of advantages over traditional confocal, one-photon fluorescence microscopy (1PFM), such as increased penetration depth (greater than 500 μm), localized excitation, and prolonged observation time [32–36]. The extra penetration depth that 2PFM affords is particularly useful for tissue imaging because surface preparation artifacts, such as damaged cells, extend >70 μm into the tissue interior, and two-photon excitation typically induces minimal photobleaching and cellular autofluorescence [36]. However, most of the one-photon (1P) fluorescent probes presently used for 2PFM have small two-photon (2P) action cross sections ($\Phi_F\,\delta_{2\mathrm{PA}}$), where Φ_F is the fluorescence quantum yield and $\delta_{2\mathrm{PA}}$ is the two-photon absorption (2PA) cross section, severely limiting their use in 2PFM. Therefore, there is a critical need for developing efficient 2PA probes that can visualize tissue and cellular morphologies deep inside the living tissues over a prolonged period of time.

2PFM significantly reduces somewhat the deleterious effects of scattering media on penetration depth due to the use of long wavelength excitation. This enables fluorescence imaging at much deeper distances than linear or confocal microscopy. 2PFM benefits from the use of near-IR wavelengths that are less prone to be scattered by tissue. The maximum imaging penetration depth within biological tissue ($z_{\max}$) has been estimated to be governed by the following relation (1) [37,38],

$$z_{\max} \approx l_s^{(\mathrm{ex})} \ln\left(\alpha P_0 \sqrt{\Phi(z_{\max})\frac{T}{\tau}}\right) \quad (1)$$

where Φ is the collection efficiency of the system (fraction of fluorescent photons detected), α is a parameter that depends on fluorophore properties and detector noise, P_0, τ, and $1/T$ are the laser average power, pulse duration, and repetition rate, respectively, and $l_s^{(\mathrm{ex})}$ is the scattering length for excitation light in tissue. The development of more efficient probes is aimed at increasing the two-photon action cross section of the probe, which ultimately increases α and consequently $z_{\max}$. In expression (1), increasing the numerical values of α would have the same effect as increasing the excitation power P_0. Experimentally, however, increasing the average excitation power may have detrimental effects on the specimen, whereas increasing fluorophore efficiency would only increase image quality. Furthermore, if a probe is efficiently excitable by 2PA and has a high fluorescence quantum yield, hence high 2P action cross section, lower concentrations are required for 2PFM, reducing its potential toxicity.

Herein, we compared the tumor-targeting characteristics of a small 2PA fluorescent bioconjugate (**1**) and a block copolymer (**3**) peptide conjugate for $\alpha_v\beta_3$ integrin imaging in tumors. The importance of multivalent RGD constructs for high affinity binding and internalization will be discussed. To investigate the use of these probes and the targeting strategy, the 2PFM *ex vivo* imaging in a Lewis Lung Carcinoma (LLC) mouse tumor model was demonstrated.

2. Materials and methods

2.1. Materials

The synthesis and characterization of fluorene-RGD conjugate **1** was described previously [39]. The syntheses of copolynorbornene **3** and **6**, and model compound **4** were also reported

[40]. The synthesis and characterization of copolynorbornene **8** is described in the supporting information. All other compounds and solvents were used as received without further purification.

2.2. Preparation of tumor-bearing mice

Lewis lung carcinoma cells were purchased from ATCC (Manassas, VA) and cultured in DMEM (Invitrogen) supplemented with 10% FBS. Experiments involving mice were done in accordance with protocols approved by the Institutional Animal Care and Use Committee. Seven-week-old male C57BL/6 mice were purchased from Harlan Laboratories (Indianapolis, IN) and acclimated for 1 week upon delivery. Each mouse was injected subcutaneously into the right flank with 3×10^6 of Lewis lung carcinoma cells suspended in 0.1 mL of PBS. Fluorene-RGD conjugate **1** or dye **2** was injected at a dose of 222 μg (66 nM) per mouse via the tail vein 10 days after the inoculation of tumor cells. Similarly copolynorbornene RGD conjuate **3** or **5** was injected at a dose of 2 nmol/g body weight (concentration was determined by the molar absorptivity coefficient of the dye). Two hours after the injection of the conjugate probe, mice were perfused with PBS and then 10% neutral-buffered formalin via the left ventricle under deep anesthesia with isoflurane. Tumors were excised and fixed with 10% neutral-buffered formalin for 18 h at 4 °C. After fixation, tumors were rinsed twice with PBS and cut into two pieces at the center of the tumors; one was used for 3D two-photon fluorescence imaging, and the other was embedded in OCT compound (Sakura Finetek, Torrance, CA) for immunohistochemistry analysis. The tumors were mounted on No.1 glass cover slips to be imaged by 2PFM.

2.3. Two-photon fluorescence microscopy of RGD small molecule conjugate 1

Two-photon fluorescence imaging for RGD conjugate **1** was performed on an Olympus IX-71 coupled to modified Fluoview FV300 laser scanning confocal microscopy system equipped with a broadband, tunable Coherent Mira Ti:sapphire laser (200 fs pulse width, 76 MHz repetition rate), pumped by a 10 W Coherent Verdi frequency doubled Nd:YAG laser. The laser was tuned to 750 nm and used as the two-photon excitation source (mode locked). The two-photon induced fluorescence was collected by a 60× or 10× microscope objective (N.A. = 1.35 and N.A. = 0.30, respectively). A high transmittance (>95%) short-pass filter (cutoff 695 nm, Semrock) was placed in front of the PMT detector within the FV300 scanhead to serve as a barrier filter to the excitation source (750 nm).

2.4. Two-photon fluorescence microscopy of RGD copolynorbornene conjugate 3

Two-photon fluorescence microscopy of the copolymer was performed on a Leica SP5 II equipped with a Coherent Chameleon Vision S laser source (prechirped compensated, 70 fs, 80 MHz). Micrographs of the whole-mounted tumors were taken under the following conditions: excitation at 750 nm, emission external non-descanned PMT detectors. A 20×, 1.0 N.A. water immersion objective was used for *ex vivo* tumor imaging.

2.5. Photostability of model compounds 2 and 4 in PBS buffer (pH = 7.4)

A solution of **2** or **4** in PBS buffer (pH = 7.4) was irradiated in 1 mm path length quartz cuvettes with a tunsten halogen lamp (LOCTITE Model 97034, average irradiance power, 60 mW), in the 400–440 nm spectral range (using glass UV–visible filters). The values of photodecomposition quantum yield, η, were calculated according to Equation (2) [41,42], and the results are the average of ten pairs of adjacent absorbance maxima.

$$\eta=\frac{(A_1-A_0)N_A}{10^3\times\varepsilon\times I\times\left[1-10^{(A_1+A_0)/2}\right](t_1-t_0)}\qquad(2)$$

where η is the photobleaching decomposition quantum yield, A_1 is absorbance maxim at t_1, A_0 is absorbance max at t_0, N_A is Avogadro's number, ε is molar absorbance in M^{-1} cm^{-1}, $t_1 - t_0$ is time exposed (s), and I is the intensity of laser in photon·$cm^{-2}s^{-1}$.

3. Results and discussion

To expand the utility of 2PA materials in a number of new areas, such as multiphoton fluorescent probes and biomarkers for biomedical applications, it is necessary to develop novel chromophores with 2PA cross sections orders of magnitude larger than endogenous chromophores in the NIR (700–1200 nm), while maintaining high fluorescence quantum yields. For this reason, there is significant motivation to carefully study the effects of molecular structure variation on two-photon processes for the design of even more efficient 2PA materials.

We demonstrated that conjugating a biological marker such as RGD to a fluorene derivative at the 9 position does not perturb the fluorenyl chromophore's electronic character responsible for efficient 2PA, since there is no alteration of the conjugation length of the chromophore [43]. Therefore, we conducted a comprehensive linear and nonlinear characterization of compound **2**, precursor of fluorene-RGD conjugate **1** (Fig. 1) [39]. The absolute values of the 2PA cross sections of compound **2**, are δ_{2PA} ~500–2500 GM at $\lambda \approx$ 700–800 nm, and Φ_F = 0.5–0.03, values that are quite suitable for 2PFM bioimaging using commercially available Ti:sapphire femtosecond lasers.

Recently, we demonstrated the covalent attachment of 2PA organic probes and RGD to a water soluble block copolymer, without affecting their photophysical properties for developing functional bioimaging probes [40]. Norbornene-based block copolymers with pendant polyethylene glycol (PEG) groups in one block, to impart hydrophilicity and biocompatibility, and succini-midyl ester groups in the other block, to facilitate covalent conjugation with a fluorescent probes, drugs or molecular markers were prepared (Fig. 2).

Another important factor in determining the efficiency of a fluorescent probe is the tendency to photobleach upon excitation, particularly under two-photon excitation. This property can easily be quantified by determining the photodecomposition quantum yield of the fluorophore. In most 2PFM techniques fluorescent probes with a low photodecomposition quantum yield, dyes that are relatively stable under excitation, are particularly useful for *in vivo* imaging where the compound is excited many times throughout the course of the experiment. In short, the ideal dye for 2PFM, for techniques that do not involve photobleaching like FRAP, will have: (1) a high 2PA cross section (δ_{2PA}) in the near IR wavelengths, preferably within the tuning range of commercial pulsed laser sources; (2) high fluorescence quantum yields (Φ_F), and (3) low decomposition quantum yields (η), which ultimately means high photostability (Table 1). With this in mind we developed a figure of merit that encompasses all of these parameters and is governed by the following relation (3) [44]:

$$\mathrm{FM}=\delta_{2PA}\cdot\Phi_F/\eta\qquad(3)$$

High photostability is an important requirement for the application of fluorescent probes in 2PFM. Photodecomposition quantum yields (η) were measured for model compounds **2** and

4 in the aqueous media. In order to measure the photostability of model compound **4** in PBS buffer, compound **4** was encapsulated in micelles using Pluronic 108 [45]. The F_M, for **2** and **4** was 119–10^{-5} and 24.93 × 10^{-5} GM in PBS buffer, respectively. These values are reasonable considering they were measured in aqueous solution.

3.1. Ex vivo two-photon fluorescence imaging after intratumor injection of small-molecule RGD conjugate 1

Direct intratumoral injection with fluorene-RGD conjugate **1** was used to assess the ability to image a “whole-mounted” tumor by 2PFM. The conjugate-injected tumors revealed fluorescence throughout most of the tumor mass, showing a concentration gradient from the injection site (Fig. 3). In this analysis, some cells exhibited a higher uptake of the fluorene-RGD conjugate **1** than others. This may be because some tumor cells express higher levels of $\alpha_v\beta_3$ integrin or because these cells have more active endocytosis taking up the dye conjugate nonspecifically. The purpose of this particular experiment was to approximate the optical penetration depths into dense tumor masses, which was approximately 70 μm with the 60× (N.A. = 1.35, oil), limited by the working distance of this high N.A. objective. Fluorescence was detected from some cytosolic organelles embedded almost 60 μm within the tissue (Fig. 4). It would indeed be difficult to extract information from the immediate inspection of the micrograph that resulted from the overlay of all the X–Y planes along the z-axis (Fig. 3). However, in micrographs resulting from the projections of successive optical planes, it is possible to clearly distinguish one cell from another and localized fluorescence within the cytosol of the cells as shown in Fig. 4.

3.2. Ex vivo two-photon fluorescence tumor vasculature imaging with small-molecule RGD conjugate 1

Fluorene-RGD conjugate **1** was used to image the vasculature of LLC tumors. Mice were injected via the tail vein with the conjugate and the tumors were excised 2 h later. The tumors were sliced in half, and one of the hemispheres was mounted, without any further treatment than fixation with formalin, for inspection under the 2PFM microscope. The other half of the tumor was sectioned and analyzed by one-photon fluorescence imaging in order to confirm the colocalization of the intravenously administered RGD conjugates with CD31 immunostaining of the sections (Fig. S4, in Supporting Information).

The potential of the *in vivo* use of the 2PA-conjugate system was demonstrated by 2PFM imaging of the whole-mounted tumor, which showed the intravenously administered conjugate **1** specifically illuminating the tumor vasculature (Figs. 5 and 6).

The 2PFM images showed the fluorene-RGD conjugate **1** remained in the vessels (i.e., extravasation was minimal). Fig. 5A was obtained from stacking all successive X–Y planes that were separated 0.3 μm along the Z axis, thus representing the entirety of the scanned volume. Stacking only 12 optical slices at a time at consecutively selected depths afforded 3.6 μm optical sections (Fig. 5B–G). These optical sections precisely exhibited the morphology of the individual vessels (vessel walls, Fig. 5B–G; and vessel lumen Fig. 5D). Reconstruction from 2PFM images of consecutive 3.6 μm sections of Fig. 5A afforded images B–G, being B and C the closest to the supporting glass. Projections of the X–Y plane along the Z axis (blue) (Fig. 5B, D and F) of 3.6 μm optical sections, show the sensitivity of the 2PFM to the focal plane of the objective. The white box in Fig. 5C, E, and G represents the entire scanned volume; whereas the green box represents the 3.6 μm section reconstructed from 12 successive 0.3 μm optical sections. Because of its high two-photon action cross section and high binding affinity to $\alpha_v\beta_3$ integrin, fluorene-RGD conjugate **1** allowed the 3D reconstruction of the tumor vessels (Fig. 5, Videos VS1–VS5 in Supporting Information). The 2PFM longitudinal-sections of these vessels were compiled, which gave a clear image of their integrity and structure (Fig. 5B–D). Furthermore, the surrounding cells were relatively "transparent" to the 750 nm irradiation, which significantly reduced the background. Micrographs obtained from stacking 0.3 μm successive layers resulted in 3D 3.6 μm optical sections that clearly showed the vessel lumen and walls (videos of reconstructed 3D images can be found in Supporting Information video VS2). These results clearly show the potential of this imaging system in evaluating detailed information on the blood vessel morphology and structure in tumors.

Supplementary video related to this article can be found at http://dx.doi.org/10.1016/j.biomaterials.2012.06.082.

Deeper image penetration into the excised tumor mass was achieved by using a smaller N.A. objective (10×, dry, N.A. = 0.30). The longer working distance of this objective allowed for probing much deeper into the tissue and the efficiency of the 2PA fluorescent probe made it possible to collect upconverted (resulting from 2PA) fluorescence without major modifications of the optical setup, or the light source. Upconverted fluorescence signals were collected from 0 to 860 μm (Fig. 6, VS3 in the Supporting Information) despite the refractive index heterogeneities and scattering that characterizes this type of tissue. Fig. 6A was made from stacking all successive X–Y planes that were along the Z axis. In Fig. 6, the orange box represents the boundaries the scanned volume. Projections of the X–Y plane along the Z axis, Y–Z plane along the X axis, and X–Z plane along the Y axis are shown in Fig. 6B, C and D, respectively. The accumulated 2PFM images show that fluorene-RGD conjugate **1** is more abundant in micro vessels than in the active vessels (Figs. 5 and 6). Moreover, the images revealed the structure of functional vessels deep within the tumor mass.

From these images, one can observe that there is little leakage of fluorene-RGD conjugate **1** from the tumor vasculature into the tumor interstitium [46]. In LLC tumors, both the tumor parenchyma (tumor cells) and the tumor vasculature (endothelium) have high integrin $\alpha_v\beta_3$ expression that can be recognized by RGD peptides. Thus, the key question is whether fluorene-RGD conjugate **1** is selectively homing to the tumor vasculature only (no extravasation needed) or also homing to the tumor parenchyma (extravasation required). Our 3D reconstruction from 2PFM images clearly indicates minimal extravasation of this probe. Indeed, well defined blood vessel walls were observed due to the probe's ability to remain bound to the endothelium of the vessels. This in turn enabled the specific imaging of tumor blood vessels. This specificity was confirmed by an excellent overlay between fluorescence of fluorene-RGD conjugate **1** and CD31 staining of the tumor sections (Fig. S4 in Supporting information). The negative controls for the 2PFM imaging consisted of mice receiving no probe (blank) as well as mice injected with dye **2** in the same concentration as the conjugate **1**. The latter served to evaluate the target specificity of conjugate **1** for integrin $\alpha_v\beta_3$. Neither control showed specific uptake that could be attributable to integrin receptors of vascular endothelial cells (Fig. S3 in Supporting information). Taken together, these results indicate that the conjugate predominantly targets the tumor vasculature through a specific RGD–integrin $\alpha_v\beta_3$ interaction without penetrating into the tumor parenchyma and interstitium.

The high Φ_F, together with the high 2PA cross section and high photostability of fluorene-RGD conjugate **1**, makes it a particularly attractive and promising imaging agent for early cancer detection, where the morphology of the tumor vasculature can be visualized and characterized using 2PFM imaging.

3.3. Ex vivo two-photon fluorescence tumor vasculature imaging with copolymer RGD conjugate 3

In the interest of comparing the performance of small-molecule RGD conjugate **1** with copolymer RGD conjugate **3**, the copolymer was injected via tail vein. The copolymer **8** was used as a negative control. As expected, both the copolymer RGD conjugate **3** and the small molecule RGD counterpart **1** revealed the vessels within the "whole-mounted" tumors. However, some differences were observed from the micrographs collected from each sample. Fig. 7A represents the images of tumor blood vessels from mice injected with copolymer **3**. A clear, uninterrupted image of the blood vessel network is observed in the X–Y projection and the 3D reconstruction (Video VS4 in Supporting Information). In contrast, the small molecule-RGD conjugate **1** exhibited significantly interrupted images of the vessel network (Fig. 7B). This important difference could be associated with the longer residence time in the circulation of the high molecular weight copolymer as well as the multivalency of the RDG peptide that increases avidity of the probe to the target $\alpha_v\beta_3$ integrin [47]. Both properties of the copolymer are expected to increase the interaction between RGD moieties and the target $\alpha_v\beta_3$ integrin molecules on the endothelium of tumor vessels. The tumor vasculature is quite heterogenous, and the level of $\alpha_v\beta_3$ integrin expression varies between the tumor vessels, possibly causing inconsistent imaging of the vessels by small molecule conjugate **1**. The block copolymer strategy significantly enhanced the sensitivity of the fluorescence imaging, illuminating the $\alpha_v\beta_3$ integrin-positive tumor vessels, which are otherwise too dim to image in deep tissues by previous RGD targeting methods. Even in the vascular cells imaged using the small molecule conjugate **1** (Fig. 7B), individual cells (presumably endothelial) can be observed while nuclei showed very little fluorescence.

The targeting specificity of the block copolymer **3** was confirmed by immunofluorescence staining of tumor sections with a CD31 antibody. Colocalization of the Alexa Fluor® 594-CD31 antibody channel (Fig. S5, red, Supporting information) with the "green" block copolymer channel validated vascular imaging by the block copolymer **3**.

4. Conclusions

The RGD peptide has been previously used as a moiety for targeting $\alpha_v\beta_3$ integrins in bioimaging and drug delivery. The versatility of this peptide was demonstrated when conjugated to a small molecule fluorophore or block copolymer of significantly higher molecular weight. These molecular weight differences exerted a difference in the sensitivity that the RGD peptide exhibits toward the integrin target. This difference may be related to the residence time in the blood stream, since higher molecular weight compounds tend to be eliminated at a slower rate. It is also expected that the multivalency of RGD peptide in the block copolymer significantly contributes to increased sensitivity of the probe through enhanced avidity toward the target integrin molecule. There is potential synergy between small-molecule probe and copolymer approaches in cancer imaging. The vascular retention of both probes yields selectivity for imaging tumor-induced angiogenesis by 2PFM. The small-molecule probe may be used when assessing integrin expression differences, whereas the block copolymer probe would be useful for imaging entire vessel networks that are functional, particularly when this needs to be done during prolonged periods of time. Therefore, both approaches may serve synergistically to provide comprehensive analysis of the vascular network in tumor tissues.

Supplementary Material

Refer to Web version on PubMed Central for supplementary material.

Acknowledgments

We wish to acknowledge the National Institutes of Health (National Institute of Biomedical Imaging and Bioengineering R15 EB008858-01 to K.B., R01 CA125255 to M.K.), the U. S. Civilian Research and Development Foundation (UKB2-2923-KV-07), and the National Science Foundation (CHE-0840431 and CHE-0832622).

References

1. Friedlander M, Theesfeld CL, Sugita M, Fruttiger M, Thomas MA, Chang S, et al. Involvement of integrins $\alpha_v\beta_3$ and $\alpha_v\beta_5$ in ocular neovascular diseases. Proc Natl Acad Sci U S A. 1996; 93:9764–9. [PubMed: 8790405]
2. Brooks PC, Clark RAF, Cheresh DA. Requirement of vascular integrin $\alpha_v\beta_3$ for angiogenesis. Science. 1994; 264:569–71. [PubMed: 7512751]
3. Gladson CL. Expression of integrin $\alpha_v\beta_3$ in small blood vessels of glioblastoma tumors. J Neuropathol Exp Neurol. 1996; 55:1143–9. [PubMed: 8939197]
4. Mikecz K. Vitaxin applied molecular evolution. Curr Opin Investig Drugs. 2000; 1:199–203.
5. Lainer DT, Brahn E. New antiangiogenic strategies for the treatment of proliferative synovitis. Expert Opin Investig Drugs. 2005; 14:1–17.
6. Ruoslahti E. RGD and other recognition sequences for integrins. Ann Rev Cell Dev Biol. 1996; 12:697–715. [PubMed: 8970741]
7. Humphries MJ. The LDV peptide motif: its role in integrin-ligand binding. Top Mol Med. 1995; 1:27–35.
8. Hirano Y, Kando Y, Hayashi T, Goto K, Nakajima A. Synthesis and cell attachment activity of bioactive oligopeptides: RGD, RGDS, RGDV and RGDT. J Biomed Mater Res. 1991; 25:1523–34. [PubMed: 1724445]
9. Dechantsreiter MA, Planker E, Matha B, Lohof E, Holzemann G, Jonczyk A, et al. N- methylated cyclic RGD peptides as highly active and selective $\alpha_v\beta_3$ integrin antagonists. J Med Chem. 1999; 42:3033–40. [PubMed: 10447947]
10. Koivunen E, Wang B, Ruoslahti E. Phage libraries displaying cyclic peptides with different ring sizes: ligand specificities of the RGD-directed integrins. Nat Biotechnol. 1995; 13:265–70.
11. Assa-Munt N, Jia X, Laakkonen P, Ruoslahti E. Solution structures and integrin binding activities of an RGD peptide with two isomers. Biochemistry. 2001; 40:2373–8. [PubMed: 11327857]
12. Dubey PK, Mishra V, Jain S, Mahor S, Vyas SP. Liposomes modified with cyclic RGD peptide for tumor targeting. J Drug Target. 2004; 12:257–64. [PubMed: 15512776]
13. Haubner R, Wester HJ, Reuning U. Radiolabelled $\alpha_v\beta_3$ integrin antagonists: a new class of tracers for tumor targeting. J Nucl Med. 1999; 40:1061–71. [PubMed: 10452325]
14. Morrison MS, Ricketts SA, Barnett J, Cuthbertson A, Tessier J, Wedge SR. Use of a novel Arg-Gly-Asp radioligand, 18F-AH111585, to determine changes in tumor vascularity after antitumor therapy. J Nucl Med. 2009; 50:116–22. [PubMed: 19091899]
15. Liu Z, Yan Y, Chin FT, Wang F, Chen X. Dual integrin and gastrin-releasing peptide receptor targeted tumor imaging using ^{18}F labeled PEGylated RGD-bombesin heterodimer ^{18}F-FB-PEG3-Glu-RGD-BBN. J Med Chem. 2009; 52:425–32. [PubMed: 19113865]
16. Scottelius M, Wester HJ. Molecular imaging targeting peptide receptors. Methods. 2009; 48:161–77. [PubMed: 19324088]
17. Zaccaro L, Del Gatto A, Pedone C, Saviano M. Peptides for tumour therapy and diagnosis: current status and future directions. Curr Med Chem. 2009; 16:780–95. [PubMed: 19275595]
18. Shah BS, Clark PA, Moioli EK, Stroscio MA, Mao JJ. Labeling of mesenchymal stem cells by bioconjugated quantum dots. Nano Lett. 2007; 7:3071–9. [PubMed: 17887799]
19. Cai W, Shin DW, Chen K, Gheysens O, Cao Q, Wang SX, et al. Peptide-labeled near - infrared quantum dots for imaging tumor vasculature in living subjects. Nano Lett. 2006; 6:669–76. [PubMed: 16608262]
20. Frangioni JV. In vivo near-infrared fluorescence imaging. Curr Opin Chem Biol. 2003; 7:626–34. [PubMed: 14580568]

21. Kim S, Lim YT, Soltesz EG, Lee J, Nakayama A. Near infrared fluorescent type II quantum dots for sentinel lymph node mapping. Nat Biotechnol. 2004; 22:93–7. [PubMed: 14661026]
22. Chen X, Conti PS, Moats RA. In vivo near-infrared fluorescence imaging of integrin $\alpha_V\beta_3$ in brain tumor xenografts. Cancer Res. 2004; 64:8009–14. [PubMed: 15520209]
23. Liu S, Hsieh WY, Jiang Y, Kim YS, Sreerama SG, Chen X, et al. Evaluation of a 99mTc- labeled cyclic RGD tetramer for noninvasive imaging integrin $\alpha_V\beta_3$-positive breast cancer. Bioconjug Chem. 2007; 18:438–46. [PubMed: 17341108]
24. Ye Y, Bloch S, Xu B, Achilefu S. Design, synthesis, and evaluation of near infrared fluorescent multimeric RGD peptides for targeting tumors. J Med Chem. 2006; 49:2268–75. [PubMed: 16570923]
25. Cheng Z, Wu Y, Xiong Z, Gambhir SS, Chen X. Near-infrared fluorescent RGD peptides for optical imaging of integrin $\alpha_V\beta_3$ expression in living mice. Bioconjug Chem. 2005; 16:1433–41. [PubMed: 16287239]
26. Schraa AJ, Kok RJ, Moorlag HE, Bos EJ, Proost JH, Meijer DK, et al. Targeting of RGD-modified proteins to tumor vasculature: a pharmacokinetic and cellular distribution study. Int J Cancer. 2002; 102:469–75. [PubMed: 12432548]
27. Mitra A, Coleman T, Borgman M, Nan A, Ghandehari H, Line BR. Polymeric conjugates of mono- and bi-cyclic $\alpha_V\beta_3$ binding peptides for tumor targeting. J Control Release. 2006; 114:175–83. [PubMed: 16889865]
28. Liu Z, Liu S, Niu G, Wang F, Liu S, Chen X. Optical imaging of integrin $\alpha_v\beta_3$ expression with near-infrared fluorescent RGD dimer with tetra (ethylene glycol) linkers. Mol Imaging. 2010; 9:21–9. [PubMed: 20128995]
29. Chen K, Xie J, Xu H, Behera D, Michalski MH, Biswal S, et al. Triblock copolymer coated iron oxide nanoparticle conjugate for tumor integrin targeting. Biomaterials. 2009; 30:6912–9. [PubMed: 19773081]
30. Williams RM, Zipfel WR, Webb WW. Multiphoton microscopy in biological research. Curr Opin Chem Biol. 2001; 5:603–8. [PubMed: 11578936]
31. Svoboda K, Yasuda R. Principles of two photon excitation microscopy and its applications to neuroscience. Neuron. 2006; 50:823–39. [PubMed: 16772166]
32. Denk W, Strickler JH, Webb WW. Two-photon laser scanning fluorescence microscopy. Science. 1990; 248:73–6. [PubMed: 2321027]
33. Helmchen F, Denk W. New developments in multiphoton microscopy. Curr Opin Neurobiol. 2002; 12:593–601. [PubMed: 12367641]
34. Cahalan MD, Parker I, Wei SH, Miller MJ. Two-photon tissue imaging: seeing the immune system in a fresh light. Nat Rev Immunol. 2002; 2:872–80. [PubMed: 12415310]
35. Zipfel WR, Williams RM, Webb WW. Nonlinear magic: multiphoton microscopy in the bioscience. Nat Biotechnol. 2003; 21:1369–77. [PubMed: 14595365]
36. Helmchen F, Denk W. Deep tissue two-photon microscopy. Nat Methods. 2005; 2:932–40. [PubMed: 16299478]
37. Oheim M, Beaurepaire E, Chaigneau E, Mertz J, Charpak S. Two-photon microscopy in brain tissue: parameters influencing the imaging depth. J Neurosci Methods. 2001; 111:29–37. [PubMed: 11574117]
38. Oheim M, Beaurepaire E, Chaigneau E, Mertz J, Charpak S. Two-photon microscopy in brain tissue: parameters influencing the imaging depth. J Neurosci Methods. 2001; 112:205.
39. Morales AR, Luchita G, Yanez CO, Bondar MV, Przhonska OV, Belfield KD. Linear and nonlinear photophysics and bioimaging of an integrin-targeting water-soluble fluorenyl probe. Org Biomol Chem. 2010; 8:2600–8. [PubMed: 20376401]
40. Biswas S, Wang X, Morales AR, Ahn HY, Belfield KD. Integrin-targeting block copolymer probes for two-photon fluorescence bioimaging. Bio-macromolecules. 2011; 12:441–9.
41. Belfield KD, Bondar MV, Przhonska OV, Schafer KJ. Photostability of a series of two photon absorbing fluorene derivatives. J Photochem Photobiol A Chem. 2004; 162:489–96.
42. Belfield KD, Bondar MV, Przhonska OV, Schafer KJ. One- and two-photon photostability of 9,9-didecyl-2,7-bis-(N, N-diphenylamino)fluorene. Photochem Photobiol Sci. 2004; 3:138–41. [PubMed: 14768631]

43. Morales AR, Yanez CO, Schafer-Hales KJ, Marcus AI, Belfield KD. Biomolecule labeling and imaging with a new fluorenyl two-photon fluorescent probe. Bioconjug Chem. 2009; 20:1992–2000. [PubMed: 19799436]
44. Wang X, Nguyen DM, Yanez CO, Rodriguez L, Ahn HY, Bondar MV, et al. High fidelity hydrophilic probe for two-photon fluorescence lysosomal imaging. J Am Chem Soc. 2010; 132:12237–9. [PubMed: 20712313]
45. Andrade CD, Yanez CO, Qaddoura MA, Wang X, Arnett CL, Coombs S, et al. Two-photon fluorescence lysosomal bioimaging with a micelle-encapsulated fluorescent probe. J Fluoresc. 2011; 21:1223–30. [PubMed: 21243414]
46. McDonald DM, Baluk P. Significance of blood vessel leakiness in cancer. Cancer Res. 2002; 62:5381–5. [PubMed: 12235011]
47. Maeda H. Tumor -selective delivery of macromolecular drugs via the EPR effect: background and future prospects. Bioconjug Chem. 2010; 21:797–802. [PubMed: 20397686]

Appendix A. Supplementary material

Supplementary data related to this article can be found, in the online version at, http://dx.doi.org/10.1016/j.biomaterials.2012.06.082.

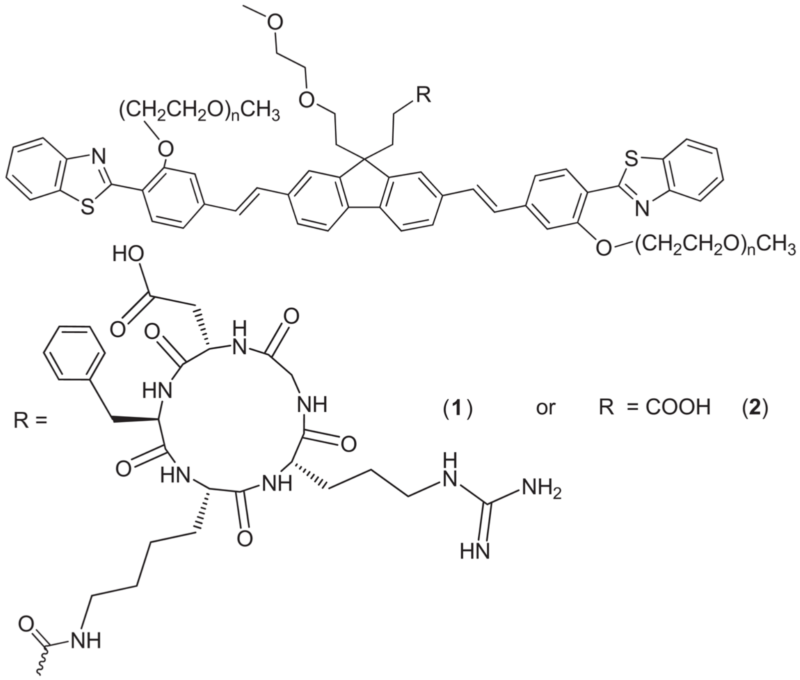

Fig. 1.

Molecular structures of fluorene-RGD conjugate **1** and control dye **2**.

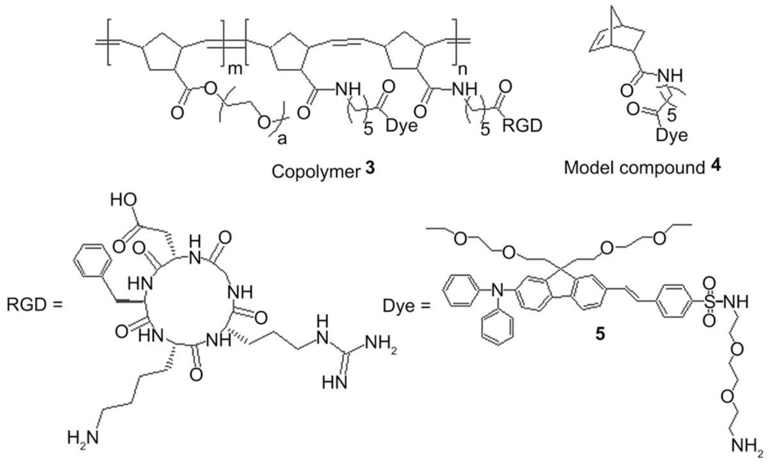

Fig. 2.
Molecular structure of multiscaffold copolynorbornene-RGD probe **3** and model compound **4**.

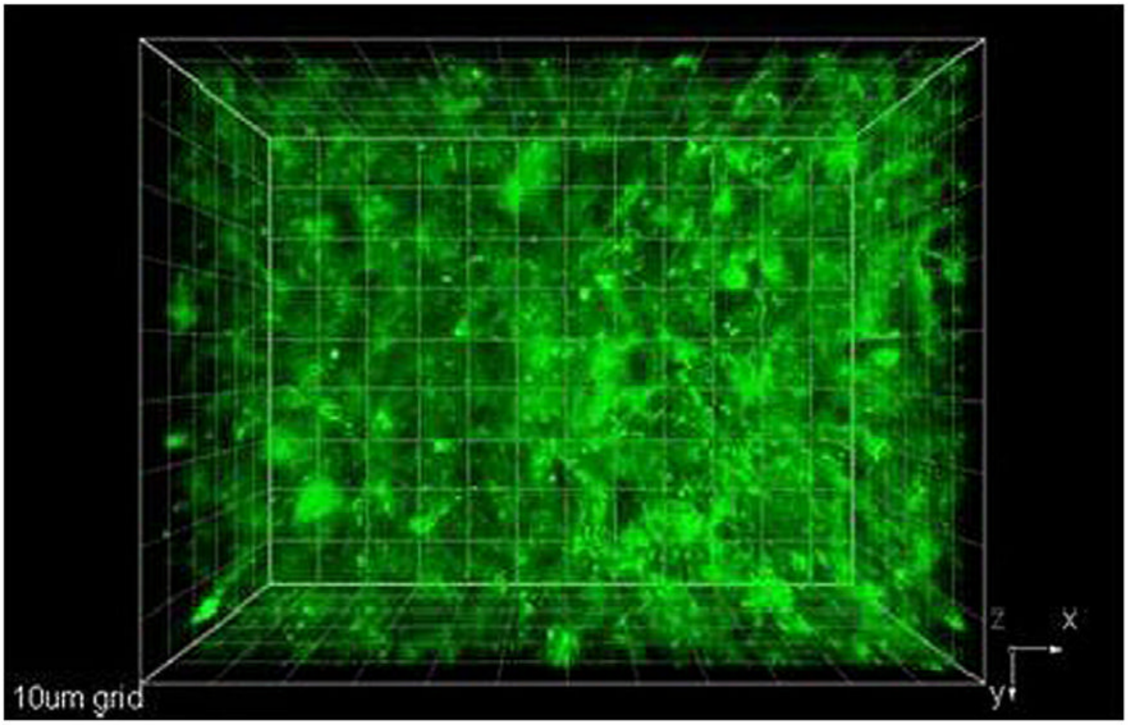

Fig. 3.

Projection of *X*–*Y* plane along the *Z* axis of a “whole-mounted” tumor. Fluorenyl-RGD conjugate 1 (66 nM) was injected intratumor. Excitation: 750 nm, 200 fs, 6 mW.

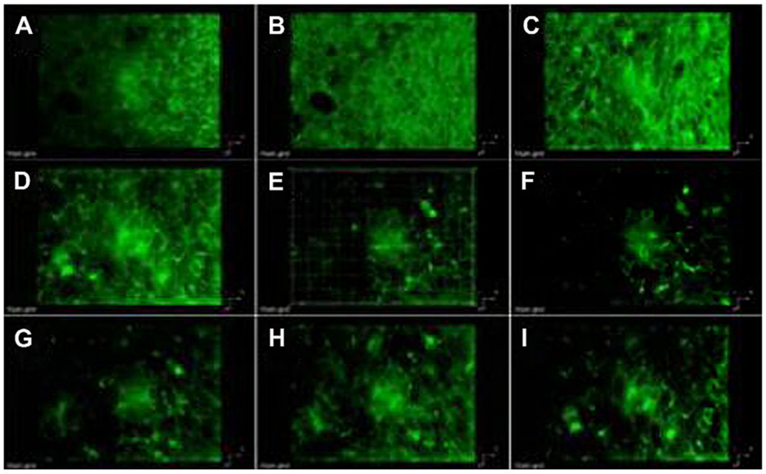

Fig. 4.

3D reconstruction from 2PFM images of consecutive 6 μm optical sections of the lung tumor from Fig. 3. A being the closest and I the furthest to the glass surface closest to the microscope objective. Excitation: 750 nm, 200 fs, 6 mW.

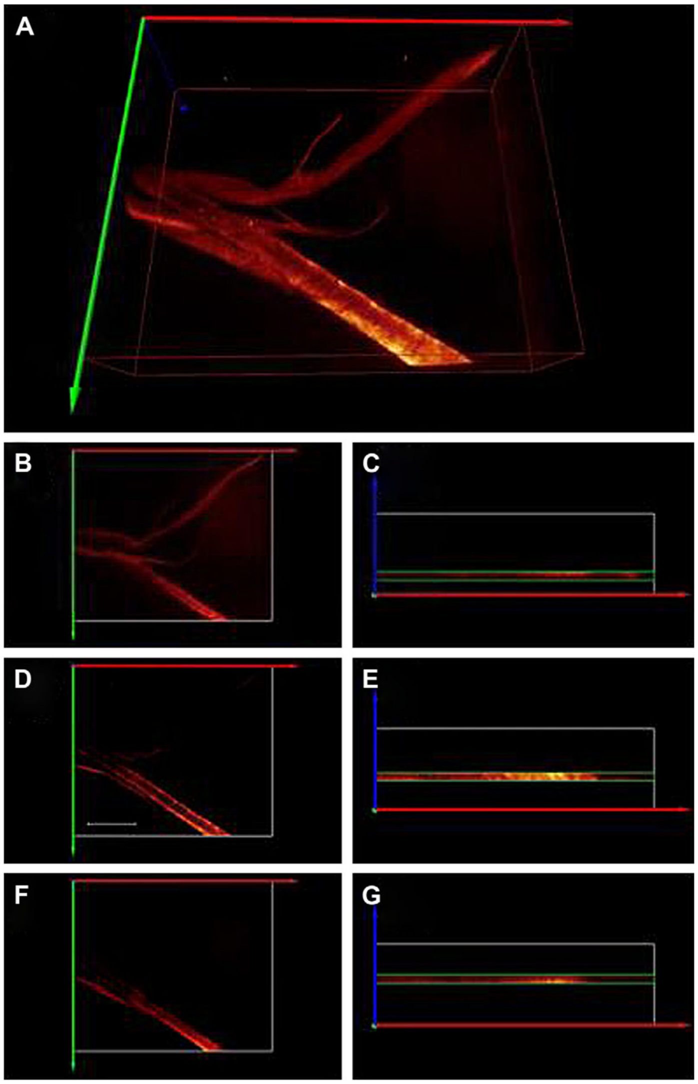

Fig. 5.

3D reconstruction from 2PFM images (0.3 μm optical sections) of LLC tumor (A). Mice received fluorene-RGD conjugate 1 (66 nM) via tail vein. Two hours later, tumors were excised for "whole mount" imaging on the 2PFM microscope. Excitation: 750 nm, 200 fs, 6 mW. Reconstruction from 2PFM images of consecutive 3.6 μm sections of A (B–G, being B and C the closest to the supporting glass). In D hollow space showing the lumen of the vessel. 5 μm scale bar (D). B, D, and F are the projections of the X–Y plane along the Z axis (blue) of 3.6 μm sections, and C, E, and G are their respective X–Z plane projections along the Y axis (green). White box in C, E, and G represents the entire scanned volume, where as the green box represents the 3.6 μm section reconstructed from 12 successive 0.3 μm optical sections. Videos showing the reconstructed vasculature networks of A and D–E can be found in the Supporting information (VS1 and VS2, respectively).

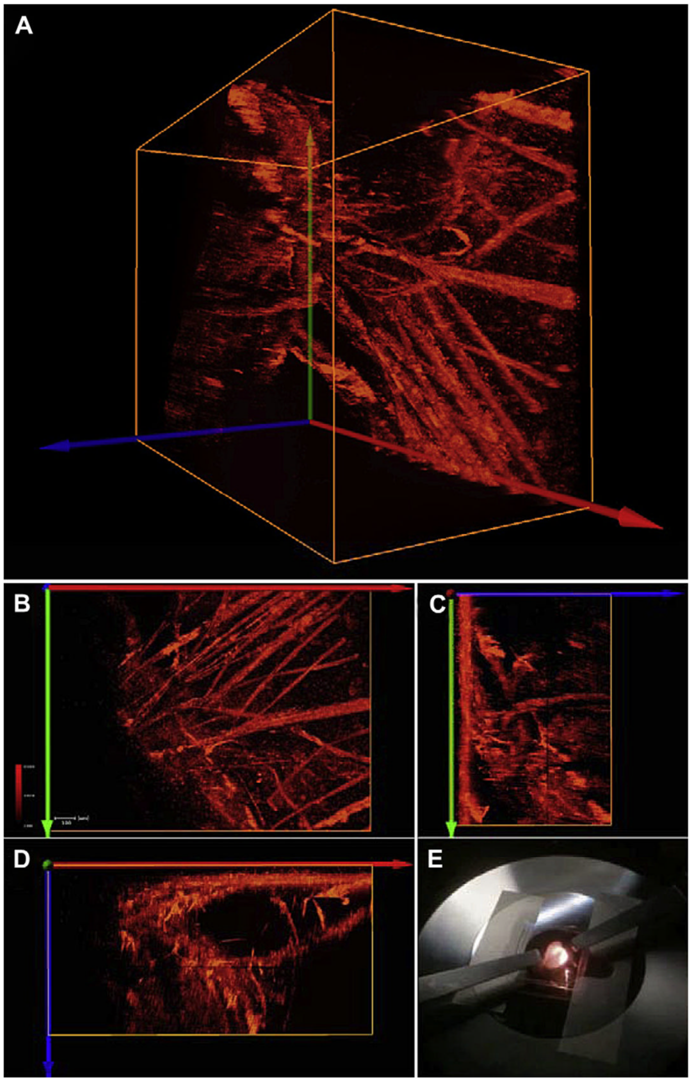

Fig. 6.

2PFM micrographs visualizing the vasculature in a whole-mounted tumor. Mouse was injected fluorene-RGD conjugate 1 (66 nM) via tail vein (G). In A the 3-D image of vasculature was made from the reconstruction of optical X–Y plane (X axis red, Y axis blue) optical slices stacked along the Y axis. Orange boxes (A–D) show the boundaries of the scanned volume within the tumor. Projections of the X–Y plane along the Z axis, Y–Z plane along the X axis, and X–Z plane along the Y axis are shown in B, C, and D, respectively. A “whole” tumor mounted on microscope stage while being scanned by 750 nm, 200 fs excitation to excite the 2PA conjugate (E). In this inverted setup the tumor was immobilized between two cover slips and scanned layer by layer from below. Upconverted (two-photon induced) epifluorescence was collected by a 10× objective. 3D reconstruction of the images was done in Amira 5.3. Tissue penetration exceeded 850 μm. Scale bar in B: 100 μm. Videos showing the reconstructed vasculature networks of A can be found in the Supporting information (VS3).

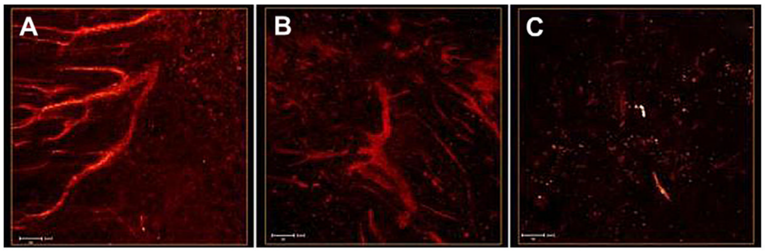

Fig. 7.

2PFM micrographs of LLC whole-mounted tumors. Mice were injected with a solution of (A) copolymer-RGD conjugate 3 (2 nmol/g body weight), (B) fluorene-RGD conjugate 1 (66 nM, B), and (C) copolymer 8 (2 nmol/g body weight) via the tail vein. All images are X–Y projections along the Z axis. Tumor vessels are clearly visualized in both A and B; however, only the copolymer conjugate offers uninterrupted images of the tumor vessel network (A). Videos showing the reconstructed vascular networks of A and B can be found in the Supporting information (VS4 and VS5, respectively).

Table 1

Photophysical parameters of compounds **2** and **4**. λ_{abs}^{max} and fluorescence λ_{fl}^{max} maxima, maximum extinction coefficients ε^{max}, fluorescence quantum yields Φ_F, fluorescence lifetimes τ, 2PA cross section δ_{2PA}, 2PA action cross section $\delta.\Phi_F$, photodecomposition quantum yield η, Figure of Merit in GM.

Compound	$\lambda_{abs}^{max} / \lambda_{fl}^{max}$	ε^{max} **10^{-3}, M^{-1} cm^{-1}**	Φ_F	τ**, ns**	δ_{2PA}	$\delta.\ \Phi_F$	η **10^5**	F_M **10^{-5},**
2	432/509 ± 1	107 ± 10	0.5 ± 0.03	1.21	800	400	3.30	121
4	393/552 ± 1	47 ± 10	0.95 ± 0.03	2.79	100	95	3.81	24